Nonlinear Dyn (2024) 112:19541–19559
https://doi.org/10.1007/s11071-024-09996-9

RESEARCH

# Dynamics of a stochastic epidemic model integrating unreported cases with a general contact susceptible function

**Ibrahim Bouzalmat**

Received: 7 May 2024 / Accepted: 8 July 2024 / Published online: 19 July 2024


**Abstract** This study investigates the qualitative properties and numerical dynamics of a stochastic epidemiological model incorporating unreported cases with a general contact susceptible function, shedding light on the intricate dynamics of infectious diseases such as COVID-19. In the qualitative analysis, we rigorously examine the mathematical properties of the model, including the existence and positivity of solutions, and identify a critical threshold parameter, $\mathcal{R}_s$, pivotal in determining the long-term behavior of the system. Notably, our analysis reveals that the stochastic noise significantly influences the dynamics, leading to distinct outcomes: if $\mathcal{R}_s$ exceeds unity, solutions converge exponentially to a unique invariant probability distribution, whereas values below one result in the extinction of infectious diseases at an exponential rate. In the numerical study, we delve into comprehensive simulations to validate our theoretical findings and explore the behavior of the model under various scenarios. Synthetic data simulations provide illustrative examples, showcasing both disease extinction and persistence phenomena. Furthermore, we investigate the impact of the susceptible contact function, $g(S)$, on disease dynamics, and propose a selection method for optimizing this function based on real-world COVID-19 data from the UK. By integrating rigorous mathematical analysis with empirical data-driven insights, our study offers valuable contributions to understanding the complex dynamics of infectious diseases.

**Keywords** Stochastic epidemic model · Population dynamics · Stochastic stability · COVID-19

## 1 Introduction

Mathematical models are indispensable tools for understanding the dynamics of infectious disease spread and for informing public health interventions. The incidence rate, an essential characteristic representing the transmission mechanism, encompasses the frequency of new infections in a susceptible population over a given period of time [1]. Stochastic epidemic models, in particular, are able to capture the randomness and variability inherent in disease transmission processes, providing a more realistic representation of epidemiological phenomena [2]. In the field of epidemiology, the principle of mass action is often applied to infectious disease models, suggesting that infection spreads via a bilinear incidence function, usually represented by $\beta SI$, where $\beta$ is the transmission rate, $S$ is the number of susceptible individuals, and $I$ is the number of infected individuals. This bilinear form assumes that each contact between a susceptible and an infected individual has an equal probability of transmitting the disease, which implies homogeneous mixing within the population [3]. However, this assumption has limitations, as it does not account for the heterogeneity

I. Bouzalmat (✉)
IMAG, CNRS, Univ Montpellier, Montpellier, France
e-mail: ibrahim.bouzalmat@umontpellier.fr

in contact patterns that can significantly affect disease transmission dynamics. Real-world interactions are influenced by various factors such as age, social behavior, and community structure, which can lead to different transmission rates among different groups within the population [4,5]. Moreover, the principle of mass action does not consider the varying intensity and duration of contacts, which can also impact the likelihood of transmission [6,7]. The use of a general contact function, denoted as $g(S)$, in stochastic epidemic models offers several advantages over the simple bilinear form. It allows for the incorporation of more complex and realistic patterns of contact among individuals, reflecting the heterogeneity and stratification of real-world populations. For example, $g(S)$ can be tailored to account for varying susceptibility across different population segments or changes in contact rates due to behavioral interventions. This can lead to a more accurate representation of the transmission process, improving the predictive power of the model and informing more effective intervention strategies. Additionally, a general contact function can be tailored to specific diseases and their modes of transmission, whether it be direct contact, indirect contact, or vector-borne, providing a flexible framework that can be adapted to various epidemiological scenarios [6,8–11]. By moving beyond the limitations of the principle of mass action, epidemiologists can better understand the nuances of disease spread and design targeted control measures that take into account the complex nature of human interactions and disease ecology.

In this paper, we present an extension of the traditional $SIR$ model [12–15], which only considers susceptible, infected, and recovered individuals, by adding a category for unreported cases of infection. The main purpose of the SIUR (Susceptible, Infected-reported, Unreported-infected, and Recovered) model is to gain a better picture of disease transmission by acknowledging that not all infected individuals are reported or identified, which could have a significant effect on the spread and control of an epidemic. The inclusion of an unreported infected compartment ($U$) allows us to capture the hidden spread of the disease, which is critical for understanding the full scope of an epidemic. Many infectious diseases, including COVID-19, exhibit a substantial number of asymptomatic or mildly symptomatic cases that go undetected but still contribute to transmission. This model is particularly useful for understanding the spread of infectious diseases and the impact of unreported cases on the dynamics of an epidemic. In the absence of unreported cases, several studies have investigated the dynamics of models incorporating different incidence rate functions. For example, the bilinear incidence form has been examined in studies by Lahrouz et al. [16,17] and Tornatore et al. [18]. The saturated functional response has been explored in works by Lan et al. [19] and Wang et al. [20], focusing on stationary and Turing patterns. Additionally, the frequency-dependent functional response has been studied by Li et al. [21], while other functional response forms such as the Beddington-DeAngelis response, investigated by Ji et al. [22] and Salman et al. [23], and the Crowley-Martin response, examined by Jan et al. [24] in the context of HIV dynamics, have been the focus of scholarly attention. These investigations have contributed to a deeper understanding of the dynamics described by stochastic models, shedding light on their behavior under different incidence rate specifications and enriching the body of knowledge pertaining to infectious disease modeling.

Our paper is organized as follows. In Sect. 2, we describe the proposed epidemic model and explain its infectious mechanism. We then delve into a thorough examination of the mathematical properties of our stochastic epidemiological model in Sect. 3. We explore key aspects such as the existence and positivity of solutions, as well as the identification of a critical threshold parameter, $\mathcal{R}_s$, which profoundly influences the long-term dynamics of the system. This section offers valuable insights into the fundamental behavior of infectious diseases within our model framework. Moving on to the Numerical Study Sect. 4, we embark on a detailed exploration of the dynamics of the model through numerical simulations. We begin by presenting synthetic data simulations that serve to illustrate and validate our theoretical findings, showcasing phenomena such as disease extinction and persistence. Subsequently, we delve deeper into specific aspects, including the impact of the susceptible contact function $g(S)$ and a selection method proposed for optimizing this function based on real-world scenarios. Additionally, we calibrate our model with real data detailing the daily incidence cases and the hospital admissions of COVID-19 cases in the UK. Finally, we conclude our paper by discussing potential avenues for future research, offering insights into the ongoing evolution of epidemiological modeling and its applications in addressing emerging health challenges.

## 2 The SIUR epidemic model

The SIUR model extends the traditional SIR framework by incorporating unreported cases of infection, which are crucial for understanding the full scope of disease transmission. The infectious mechanism in this model is described through the interaction between susceptible, reported infected, and unreported infected populations. The transmission rate $\beta g(S)\,(I+U)\,/1+aI^p$ reflects the likelihood of susceptible individuals contracting the disease based on the combined presence of reported and unreported infected individuals. This formulation allows the model to capture the effects of underreporting on the overall dynamics of disease spread, highlighting the significant impact of unreported cases on public health strategies. The model consists of the following set of nonlinear stochastic differential equations:

$$\begin{cases} dS &= \left[\mu_1 - \mu_1 S - \beta g(S)\frac{(I+U)}{1+aI^p} + \omega R\right]dt \\ &\quad -\sigma g(S)\frac{(I+U)}{1+aI^p}dB(t), \\ dI &= \left[-(\mu_1+\alpha+\delta)I + \nu\beta g(S)\frac{(I+U)}{1+aI^p}\right]dt \\ &\quad +\sigma\nu g(S)\frac{(I+U)}{1+aI^p}dB(t), \\ dU &= \left[-(\mu_1+\alpha+\delta)U + (1-\nu)\beta g(S)\frac{(I+U)}{1+aI^p}\right]dt \\ &\quad +\sigma(1-\nu)g(S)\frac{(I+U)}{1+aI^p}dB(t), \\ dR &= [-(\mu_1+\omega)R + \delta(I+U)]\,dt. \end{cases} \tag{1}$$

The positive constants $\mu, \alpha, \delta$, and $\omega$ denote birth and death rates, disease-induced death, recovery rates for both reported and unreported infected individuals, and the rate of losing immunity, respectively. The expression $\beta g(S)\,(I+U)\,/1+aI^p$ signifies the rate at which susceptible individuals contract the infection, considering factors like transmission rate ($\beta$), general contact function ($g(S)$), and the combined impact of reported ($I$) and unreported ($U$) infected individuals. The denominator $1+aI^p$ adjusts the infection rate based on reported cases, with $a$ and $p$ being positive constants that modulate the influence of reported infections on transmission. The parameter $\nu$ indicates the proportion of new infections that are reported. The function $g$ is subject to the conditions $g(S) \geq 0$ and being continuously differentiable with $g(0) = 0$. Additionally, the Brownian motion is denoted by $B(t)$, and $\sigma > 0$ represents the intensity of environmental noise affecting the infection coefficient $\beta$.

The SDE (1) can alternatively be formulated using the approach outlined in literature [25]. Given any initial value $z_0 := Z(0) = (s, i, u, r)$ and a sufficiently small time increment $\Delta t \geq 0$, we posit that the solution $Z(t) = (S(t), I(t), U(t), R(t))$ forms a Markov process with a conditional mean and a conditional variance respectively given by

$$\begin{aligned} &\mathbb{E}[Z(t+\Delta t) - Z(t) \mid Z = Z(0)] \\ &\approx \begin{bmatrix} \mu_1 - \mu_1 S - \beta g(S)\frac{(I+U)}{1+aI^p} + \omega R \\ -(\mu_1+\alpha+\delta)I + \nu\beta g(S)\frac{(I+U)}{1+aI^p} \\ -(\mu_1+\alpha+\delta)U + (1-\nu)\beta g(S)\frac{(I+U)}{1+aI^p} \\ -(\mu_1+\omega)R + \delta(I+U) \end{bmatrix}\Delta t, \end{aligned}$$

and

$$\begin{aligned} &\mathrm{Var}[Z(t+\Delta t) - Z(t) \mid Z = Z(0)] \\ &\approx \begin{bmatrix} \sigma^2 g(S)^2\left(\frac{(I+U)}{1+aI^p}\right)^2 \\ \sigma^2\nu^2 g(S)^2\left(\frac{(I+U)}{1+aI^p}\right)^2 \\ \sigma^2(1-\nu)^2 g(S)^2\left(\frac{(I+U)}{1+aI^p}\right)^2 \\ 0 \end{bmatrix}\Delta t. \end{aligned}$$

## 3 Qualitative properties of the model

In this study, we will begin by assuming the standard conditions for a probability space $\mathbb{S} = (\Gamma, \mathcal{F}, \{\mathcal{F}_t\}_{t\geq 0}, \mathbb{P})$, incorporating the prerequisites of being increasing and right-continuous. Furthermore, we will posit that the filtration $\{\mathcal{F}_t\}_{t\geq 0}$ encompasses all $\mathbb{P}$-null sets in its initial set of events, denoted by $\mathcal{F}_0$. We define $\mathbb{R}^4_+ := [0,\infty)^4$ to represent the non-negative real space. To delve into the analysis of the model represented by the system (1), we first delineate the boundaries of a set denoted as $\Omega$, which can be described as follows:

$$\Omega = \left\{X \in \mathbb{R}^4_+;\ \frac{\mu_1}{\mu_1+\alpha} < X_1 + X_2 + X_3 + X_4 < 1\right\}.$$

Next, we present the following theorem.

**Theorem 1** *The subsequent results are established.*

i) *For any $z_0 \in \Omega$, there exists a unique global solution to the SDE (1), such that*

$$\mathbb{P}\{Z(t) = (S(t), I(t), U(t), R(t)) \in \Omega \ \ \forall t \geq 0\} = 1, \quad a.s..$$

ii) *For any $\theta > 0$, there exist two positive constants $C_1$ and $C_2$ such that the solution $Z(t)$ of the system (1) satisfies:*

$$\mathbb{E}\left[(S(t)+I(t)+U(t)+R(t))^{\theta+1}\right] \leq \left((s+i+u+r)^{\theta+1}-\frac{C_2}{C_1}\right)e^{-C_1 t}+\frac{C_2}{C_1}. \tag{2}$$

*Proof* $i$) The set $\Omega$ is almost surely positively invariant under the dynamics of system (1). This assertion follows from standard arguments, and a detailed proof can be found in [14,26].
For $ii$), we introduce the Lyapunov function

$$\psi_1(S,I,U,R) = (S+I+U+R)^{\theta+1},$$

where the parameter $\theta > 0$ will be determined subsequently. Calculating the differential operator associated with system (1), we obtain

$$\begin{aligned}\mathcal{L}\psi_1 &= (\theta+1)(S+I+U+R)^{\theta}\\ &\quad(\mu_1-\mu_1(S+I+U+R)-\alpha(I+U))\\ &\quad+\frac{\theta(\theta+1)}{2}(S+I+U+R)^{\theta-1}\sigma^2 g(S)^2\\ &\quad\left(\frac{(I+U)}{1+aI^p}\right)^2\\ &\leq \mu_1(\theta+1)(S+I+U+R)^{\theta}+(\theta+1)\\ &\quad(S+I+U+R)^{\theta-1}\left(-\mu_1(S+I+U+R)^2\right.\\ &\quad\left.+\frac{\theta}{2}\sigma^2 g(S)^2\left(\frac{(I+U)}{1+aI^p}\right)^2\right).\end{aligned}$$

Define $M = \sup_{(S,I,U,R)} \frac{g(S)^2(I+U)^2}{(1+aI^p)^2(S+I+U+R)^2}$, we get:

$$\begin{aligned}\mathcal{L}\psi_1 &\leq \mu_1(\theta+1)(S+I+U+R)^{\theta}+(\theta+1)\\ &\quad\left(-\mu_1+\frac{\theta}{2}\sigma^2 M\right)\psi_1.\end{aligned} \tag{3}$$

Now, choosing $\theta < \frac{2\mu_1}{\sigma^2 M}$, we let $C_1 := \mu_1 - \frac{\theta}{2}\sigma^2 M$ and

$$\begin{aligned}C_2 := \sup_{(S,I,U,R)} &\left\{\mu_1(\theta+1)(S+I+U+R)^{\theta}\right.\\ &\left.-\theta C_1(S+I+U+R)^{\theta+1}\right\}.\end{aligned}$$

We deduce from (3) that

$$\mathcal{L}\psi_1(S,I,U,R)+C_1\psi_1(S,I,U,R) \leq C_2 < +\infty. \tag{4}$$

Define the stopping time $\tau_\varepsilon = \inf\{t \geq 0, S(t)+I(t)+U(t)+R(t) \geq \varepsilon\}$. Using (4) and the Itô formula, we have

$$\begin{aligned}&\mathbb{E}\left[e^{C_1(t\wedge\tau_\varepsilon)}\psi_1(S(t\wedge\tau_\varepsilon),I(t\wedge\tau_\varepsilon),U(t\wedge\tau_\varepsilon),R(t\wedge\tau_\varepsilon))\right]\\ &= \psi_1(s,i,u,r)+\mathbb{E}\left[\int_0^{t\wedge\tau_\varepsilon} e^{C_1 v}[\mathcal{L}\psi_1(S(v),I(v),\right.\\ &\quad\left.U(v),R(v))+C_1\psi_1(S(v),I(v),U(v),R(v))]dv\right]\\ &\leq \psi_1(s,i,u,r)+\frac{C_2}{C_1}\left(e^{C_1 t\wedge\tau_\varepsilon}-1\right).\end{aligned}$$

Letting $\varepsilon \to +\infty$ and applying the Fatou Lemma we get

$$\mathbb{E}\left[(S(t)+I(t)+U(t)+R(t))^{\theta+1}\right] \leq \left((s+i+u+r)^{\theta+1}-\frac{C_2}{C_1}\right)e^{-C_1 t}+\frac{C_2}{C_1}.$$

The proof is now complete. □

Next, we aim to analyze the dynamics of the stochastic system (1). To proceed, we define the following threshold:

$$\mathcal{R}_s = \frac{\beta M_s}{\mu_1+\alpha+\delta+\frac{1}{2}\sigma^2\frac{M_s^2}{(1+a)^2}},$$

where $M_s = \sup_{S\in(0,1)} g(S)$.
Initially, we will demonstrate that if the stochastic threshold $\mathcal{R}_s$ is greater than 1, then for any initial solution $z_0 \in \Omega$, the probability distribution of the solution $Z(t)$ converges exponentially to an invariant distribution $\pi \in \Omega$. In other words, the levels of susceptible, infected, unreported, and recovered individuals reach a stable positive state eventually. For this purpose, let?s define $\|\cdot,\cdot\|_{TV}$ to be the total variation norm on the space $(\mathbb{R}_+^n, \mathcal{B}(\mathbb{R}_+^n))$ as:

$$\|\phi,\varphi\|_{TV} = \sup_{A\in\mathcal{B}(\mathbb{R}_+^n)} |\phi(A)-\varphi(A)|,$$

where $\mathcal{B}(\mathbb{R}_+^n)$ denotes the Borel measurable subsets of $\mathbb{R}_+^n$.

**Theorem 2** *For all initial values $z_0 \in \Omega$. If $\mathcal{R}_s > 1$ and $\beta > \frac{1}{2}\sigma^2 M_s$, then there exists an invariant probability measure $\pi$ on $\Omega$ and $\eta > 0$ such that*

$$\lim_{t\to\infty} e^{\eta t}\|P(t,z_0,\cdot)-\pi(\cdot)\|_{TV} = 0,$$

*where $P(t,z_0,\cdot)$ is the transition probability of $Z(t)$ starting from $z_0$.*

*Proof* Consider the Lyapunov function

$$\psi_2(S, I, U, R) = (I + U)^{k_0}.$$

By the Itô formula, we get

$$\begin{aligned} d\psi_2 &= k_0 (I+U)^{k_0} \left( -(\mu_1 + \alpha + \delta) + \beta \frac{g(S)}{1+aI^p} \right. \\ &\quad \left. + \frac{1}{2}(k_0 - 1)\sigma^2 \frac{g^2(S)}{(1+aI^p)^2} \right) dt \\ &\quad + k_0 (I+U)^{k_0} \sigma \frac{g(S)}{1+aI^p} dB_t \\ &\leq k_0 (I+U)^{k_0} \left( -(\mu_1 + \alpha + \delta) + \beta M_s \right. \\ &\quad \left. + \frac{1}{2}|k_0 - 1|\sigma^2 M_s^2 \right) dt + k_0 (I+U)^{k_0} \sigma M_s dB_t \\ &:= C_3 \psi_2 dt + k_0 \sigma M_s \psi_2 dB_t, \end{aligned} \tag{5}$$

where $C_3 = k_0 \left( -(\mu_1 + \alpha + \delta) + \beta M_s + \frac{1}{2}|k_0 - 1| \sigma^2 M_s^2 \right)$ and in the last inequality we use the fact that $(1 + aI^p) \geq 1$.

By integrating Eq.(5), followed by taking the expectation on both sides and applying the well-known Gronwall inequality, we derive the following result:

$$\mathbb{E}\left(\psi_2(S, I, U, R)\right) \leq \psi_2(s, i, u, r)\, e^{C_3 t}. \tag{6}$$

On the other hand and through the Itô formula, we have

$$ln\left(I(t) + U(t)\right) = ln\left(i + u\right) - G(t), \tag{7}$$

where

$$\begin{aligned} G(t) &= -\int_0^t \mathcal{L}\left(ln(I(v) + U(v))\right) dv \\ &\quad - \int_0^t \sigma \frac{g(S)}{1+aI^p} dB_v, \end{aligned}$$

and $\mathcal{L}\left(ln(I+U)\right)$ is given by

$$\begin{aligned} &\mathcal{L}\left(ln(I+U)\right) = -(\mu_1 + \alpha + \delta) + \beta \frac{g(S)}{1+aI^p} \\ &\quad - \frac{1}{2}\sigma^2 \frac{g^2(S)}{(1+aI^p)^2} \\ &= \beta M_s - (\mu_1 + \alpha + \delta) - \frac{1}{2}\frac{\sigma^2 M_s^2}{(1+a)^2} + \beta \frac{g(S)}{1+aI^p} \\ &\quad - \frac{1}{2}\sigma^2 \frac{g^2(S)}{(1+aI^p)^2} - \beta M_s + \frac{1}{2}\frac{\sigma^2 M_s^2}{(1+a)^2} \\ &= \beta M_s \left(1 - \frac{1}{\mathcal{R}_0}\right) + \frac{g(S)}{1+aI^p} \left(\beta - \frac{1}{2}\sigma^2 \frac{g(S)}{1+aI^p}\right) \\ &\quad + \frac{1}{2}\frac{\sigma^2}{(1+a)^2} \left(M_s - \frac{(1+a)^2\beta}{\sigma^2}\right)^2 + \frac{1}{2}\frac{(1+a)^2\beta^2}{\sigma^2}. \end{aligned}$$

Since $1 + aI^p \geq 1$, $g(S) \leq M_s$, and $\beta > \frac{1}{2}\sigma^2 M_s$, we conclude that

$$\begin{aligned} \mathcal{L}\left(ln(I+U)\right) &\geq \beta M_s \left(1 - \frac{1}{\mathcal{R}_0}\right) + \frac{g(S)}{1+aI^p} \\ &\quad \left(\beta - \frac{1}{2}\sigma^2 M_s\right) \\ &\geq \beta M_s \left(1 - \frac{1}{\mathcal{R}_s}\right) := C_4 > 0. \end{aligned}$$

Hence, there exists a $t_0 > 0$ such that for any $T > t_0$ we have

$$\mathbb{E}\left[G(T)\right] \leq -C_4 T. \tag{8}$$

From Eqs. (6) and (7), we derive

$$\begin{aligned} &\mathbb{E}\left[e^{2G(T)}\right] + \mathbb{E}\left[e^{-2G(T)}\right] = (i+u)^2\, \mathbb{E}\left[(I+U)^{-2}\right] \\ &\quad + (i+u)^{-2}\, \mathbb{E}\left[(I+U)^2\right] \\ &\leq 2e^{C_3 T}. \end{aligned}$$

Using [27, Lemma 3.4], then the log-Laplace transform $ln\mathbb{E}\left[e^{\theta G(T)}\right]$ satisfies the following equation

$$ln\mathbb{E}\left[e^{\theta G(T)}\right] \leq \theta \mathbb{E}\left[G(T)\right] + \theta^2 C_5, \quad \theta \in [0, 1), \tag{9}$$

for some $C_5 < \infty$.

By considering $\theta$ to be sufficiently small, it can be inferred from Eqs. (8) and (9) that

$$\mathbb{E}\left[e^{\theta G(T)}\right] \leq e^{-\theta C_4 T},$$

and

$$\begin{aligned} &\mathbb{E}\left[(I(T) + U(T))^{-\theta}\right] \\ &\quad \leq (i+u)^{-\theta} e^{-\theta C_4 T}, \quad \theta \in [0, 1). \end{aligned} \tag{10}$$

Now, consider the Lyaunouv $C^2$-function

$$\begin{aligned} \psi_3(S, I, U, R) &= \psi_1(S, I, U, R) + \psi_2(S, I, U, R), \\ &\theta \in [0, 1). \end{aligned}$$

Then, using (2) and Eq.(10), we can deduce that

$$\begin{aligned} &\mathbb{E}\left(\psi_3\left(S(T), I(T), U(T), R(T)\right)\right) \\ &\quad = \mathbb{E}\left(\psi_1\left(S(T), I(T), U(T), R(T)\right)\right) \\ &\quad + \mathbb{E}\left(\psi_2\left(S(T), I(T), U(T), R(T)\right)\right) \\ &\leq \left(\psi_1(s, i, u, r) - \frac{C_2}{C_1}\right) e^{-C_1 T} \end{aligned}$$

$$+\frac{C_2}{C_1}+\psi_2(s,i,u,r)e^{-\theta C_4 T}$$
$$\leq \xi_T\psi_3(s,i,u,r)+\frac{C_2}{C_1}\left(1-e^{-C_1T}\right),$$

where $\xi_T = max\{e^{-C_1T}, e^{-\theta C_4 T}\}$ and $\lim_{T\to\infty}\xi_T = 0$.

Given that the Markov process $(S(t), I(t), U(t), R(t))$ is irreducible, and the transition probability function $P(t, z_0, \cdot)$ possesses a smooth density, it can be deduced from [28,29] that there exist positive constants $\eta > 0$ and $C > 0$ such that

$$\|P(t,z_0,\cdot)-\pi(\cdot)\|_{TV} \leq C\psi_3(s,i,u,r)e^{-\eta t}.$$

Moreover, letting $t \to \infty$, we get

$$\lim_{t\to\infty}\|P(t,z_0,\cdot)-\pi(\cdot)\|_{TV} = 0.$$

Therefore, the proof is completed. □

Subsequently, our objective is to establish the stochastic asymptotic stability of the disease-free equilibrium $E_0 = (1, 0, 0, 0)$ of system (1) when the threshold $\mathcal{R}_s$ is less than 1. Additionally, we aim to demonstrate that under this condition, the population sizes of infected, unreported, and recovered individuals exponentially diminish to zero, while the population of susceptible individuals eventually stabilizes at a positive level.

**Theorem 3** *Consider the stochastic system (1) with initial condition in Ω. If $\mathcal{R}_s < 1$ and $M_s\sigma^2 < \beta(1+a)^2$, then the following results hold:*

i) *The disease-free equilibrium $E_0$ of (1) is stochastically asymptotically stable.*
ii) *$I(t)$, $U(t)$ and $R(t)$ tend to zeros exponentially with probability 1, i.e.,*

$$\lim_{t\to\infty} I(t) = \lim_{t\to\infty} U(t) = \lim_{t\to\infty} R(t) = 0, \quad a.s.,$$

*and*

$$\lim_{t\to\infty} S(t) = 1, \quad a.s.$$

*Proof i)* Let $z_0 \in \Omega$. Introduce the positive-definite function

$$\psi_3(S,I,U,R) = \frac{1}{2}\theta_1(1-S)^2+\frac{1}{k}(I+U)^k+\frac{1}{2}\theta_2R^2,$$

where $\theta_1, \theta_2$ and $k$ are real positive constants to be chosen carefully later on. We have

$$\begin{aligned}\mathcal{L}\psi_3 = &-\mu_1\theta_1(1-S)^2+\theta_1\beta\frac{g(S)}{1+aI^p}(I+U)(1-S)-\omega\theta_1R(1-S)\\&+\frac{1}{2}\theta_1\sigma^2\frac{g^2(S)}{(+aI^p)^2}(I+U)^2-(\mu_1+\alpha+\delta)(I+U)^k+\beta\frac{g(S)}{1+aI^p}(I+U)^k\\&+\frac{1}{2}(k-1)\sigma^2\frac{g^2(S)}{(1+aI^p)^2}(I+U)^k-\theta_2(\mu_1+\omega)R^2+\theta_2\delta(I+U)R.\end{aligned}$$

Using $g(S) \leq M_s$, $1 \leq 1+aI^p \leq 1+a$, and $I+U \leq 1-S$, we estimate

$$\begin{aligned}\mathcal{L}\psi_3 \leq &-\mu_1\theta_1(1-S)^2+\theta_1\beta M_s(I+U)(1-S)-\omega\theta_1R(I+U)+\frac{1}{2}\theta_1\sigma^2M_s^2(I+U)^2\\&-(\mu_1+\alpha+\delta)(I+U)^k+\beta g(S)(I+U)^k-\frac{1}{2}\sigma^2\frac{g^2(S)}{(1+a)^2}(I+U)^k+\frac{k}{2}\sigma^2M_s^2(I+U)^k\\&-\theta_2(\mu_1+\omega)R^2+\theta_2\delta(I+U)R.\end{aligned}$$

Selecting $k \in (0, 2)$, and employing that

$$(I+U)(1-S) \leq \frac{\varepsilon}{2}(1-S)^2+\frac{1}{2\varepsilon}(I+U)^k, \quad \text{for all } \varepsilon > 0,$$

we get

$$\begin{aligned}\mathcal{L}\psi_3 \leq &-\theta_1\left(\mu_1-\frac{\varepsilon}{2}\beta M_s\right)(1-S)^2\\&+\Bigg(-(\mu_1+\alpha+\delta)+\beta g(S)\\&+-\frac{1}{2}\sigma^2\frac{g^2(S)}{(1+a)^2}+\frac{k}{2}\sigma^2M_s^2\\&\frac{1}{2}\theta_1\left(\frac{\beta M_s}{2\varepsilon}+\sigma^2M_s^2\right)\Bigg)(I+U)^k\\&-\theta_2(\mu_1+\omega)R^2+(\theta_2\delta-\theta_1\omega)(I+U)R\\:= &-\theta_1\left(\mu_1-\frac{\varepsilon}{2}\beta M_s\right)(1-S)^2\\&+\Bigg(\varphi(g(S))+\frac{k}{2}\sigma^2M_s^2\\&+\frac{1}{2}\theta_1\left(\frac{\beta M_s}{2\varepsilon}+\sigma^2M_s^2\right)\Bigg)(I+U)^k\\&-\theta_2(\mu_1+\omega)R^2+(\theta_2\delta-\theta_1\omega)(I+U)R,\end{aligned}$$

where $\varphi(X) = -\frac{1}{2}\frac{\sigma^2}{(1+a)^2}X^2+\beta X-(\mu_1+\alpha+\delta)$. From the assumption $M_s\sigma^2 < \beta(1+a)^2$, it's straightforward to verify that $\varphi(X)$ is increasing on $(0, M_s)$. Thus,

$$\varphi(g(S)) \leq \varphi(M_s) = \beta M_s\left(1-\frac{1}{\mathcal{R}_s}\right) < 0.$$

Thereby, we can choose $\theta_1, \theta_2$ and $\varepsilon$ such that

$$\mu_1 - \frac{\varepsilon}{2}\beta M_s > 0, \quad \beta M_s\left(1-\frac{1}{\mathcal{R}_s}\right) + \frac{k}{2}\sigma^2 M_s^2 + \frac{1}{2}\theta_1\left(\frac{\beta M_s}{2\varepsilon} + \sigma^2 M_s^2\right) < 0,$$

and

$$\theta_2\delta - \theta_1\omega < 0.$$

Hence,

$$\mathcal{L}\psi_3 \leq 0.$$

Therefore, the equilibrium state $E_0$ is stochastically stable for system (1).

*ii*) By the Itô formula, we derive from the second and third equations of system (1)

$$dln\,(I(t)+U(t)) = \mathcal{L}\,(ln\,(I(t)+U(t)))\,dt + \sigma\frac{g(S)}{1+aI^p}dB_t, \tag{11}$$

where

$$\begin{aligned}\mathcal{L}\,(ln(I+U)) &= -(\mu_1+\alpha+\delta) + \beta\frac{g(S)}{1+aI^p} - \frac{1}{2}\sigma^2\frac{g^2(S)}{(1+aI^p)^2}\\ &\leq -(\mu_1+\alpha+\delta) + \beta g(S) - \frac{1}{2}\frac{\sigma^2}{(1+a)^2}g^2(S)\\ &:= \varphi(g(S)).\end{aligned}$$

Since,

$$\varphi(g(S)) \leq \varphi(M_s) = \beta M_s\left(1-\frac{1}{\mathcal{R}_s}\right).$$

Consequently,

$$\mathcal{L}\,(ln(I+U)) \leq \beta M_s\left(1-\frac{1}{\mathcal{R}_s}\right) := C_5. \tag{12}$$

Integrating Eq. (11) from 0 to $t$, considering (12), taking expectations, and dividing by $t$ on both sides, we obtain

$$\frac{ln\,(I(t)+U(t))}{t} \leq \frac{ln\,(i+u)}{t} + C_5 + \frac{1}{t}\int_0^t \sigma\frac{g(S)}{1+aI^p}dB_v. \tag{13}$$

Given that $g(S) \leq M_s$ and $1+aI^p \geq 1$, and employing the law of large numbers for martingales, we deduce

$$\limsup_{t\to\infty}\frac{1}{t}\int_0^t \sigma\frac{g(S)}{1+aI^p}dB_v = 0 \quad a.s.$$

Therefore,

$$\limsup_{t\to\infty}\frac{ln\,(I(t)+U(t))}{t} \leq C_5 < 0 \quad a.s.,$$

which ensures

$$\lim_{t\to\infty} I(t) = \lim_{t\to\infty} U(t) = 0 \quad a.s. \tag{14}$$

The remaining steps of the proof follow a similar approach as used in [14,30,31].

The proof is thus concluded successfully. □

## 4 Numerical study

In this section, we delve into the numerical investigation of our study, providing a comprehensive analysis of the dynamics of the proposed model under various scenarios. We use the Milstein higher-order approach [32] to implement a numerical sheme of the system. We examine the impact of crucial parameters, including the infection force characterized by $p$, and the choice of the susceptible contact function $g(S)$, across synthetic and real datasets. The discretization scheme of the system (1) takes the following form:

$$\begin{cases}
\begin{aligned}
S_{k+1} &= S_k + \big(\mu_1 - \mu_1 S_k - \beta g(S_k)\tfrac{(I_k+U_k)}{1+aI_k^p} + \omega R_k\big)h\\
&\quad -\sigma g(S_k)\tfrac{(I_k+U_k)}{1+aI_k^p}\eta_k\sqrt{h}\\
&\quad -\tfrac{\sigma^2}{2}g(S_k)\tfrac{(I_k+U_k)}{1+aI_k^p}\left(\eta_k^2-1\right)h,\\
I_{k+1} &= I_k + \big(-(\mu_1+\alpha+\delta)I_k + \nu\beta g(S_k)\tfrac{(I_k+U_k)}{1+aI_k^p}\big)h\\
&\quad +\sigma\nu g(S_k)\tfrac{(I_k+U_k)}{1+aI_k^p}\eta_k\sqrt{h}\\
&\quad +\tfrac{\sigma^2}{2}\nu g(S_k)\tfrac{(I_k+U_k)}{1+aI_k^p}\left(\eta_k^2-1\right)h,\\
U_{k+1} &= U_k + \big(-(\mu_1+\alpha+\delta)\\
&\quad U_k + (1-\nu)\beta g(S_k)\tfrac{(I_k+U_k)}{1+aI_k^p}\big)h\\
&\quad +\sigma(1-\nu)g(S_k)\tfrac{(I_k+U_k)}{1+aI_k^p}\eta_k\sqrt{h}\\
&\quad +\tfrac{\sigma^2}{2}(1-\nu)g(S_k)\tfrac{(I_k+U_k)}{1+aI_k^p}\left(\eta_k^2-1\right)h,\\
R_{k+1} &= R_k + \big(-(\mu_1+\omega)R_k + \delta(I_k+U_k)\big)h.
\end{aligned}
\end{cases}$$

where $\eta_k$ are mutually independent $N(0,1)$ random variables for $k = 1, 2, \cdots$.

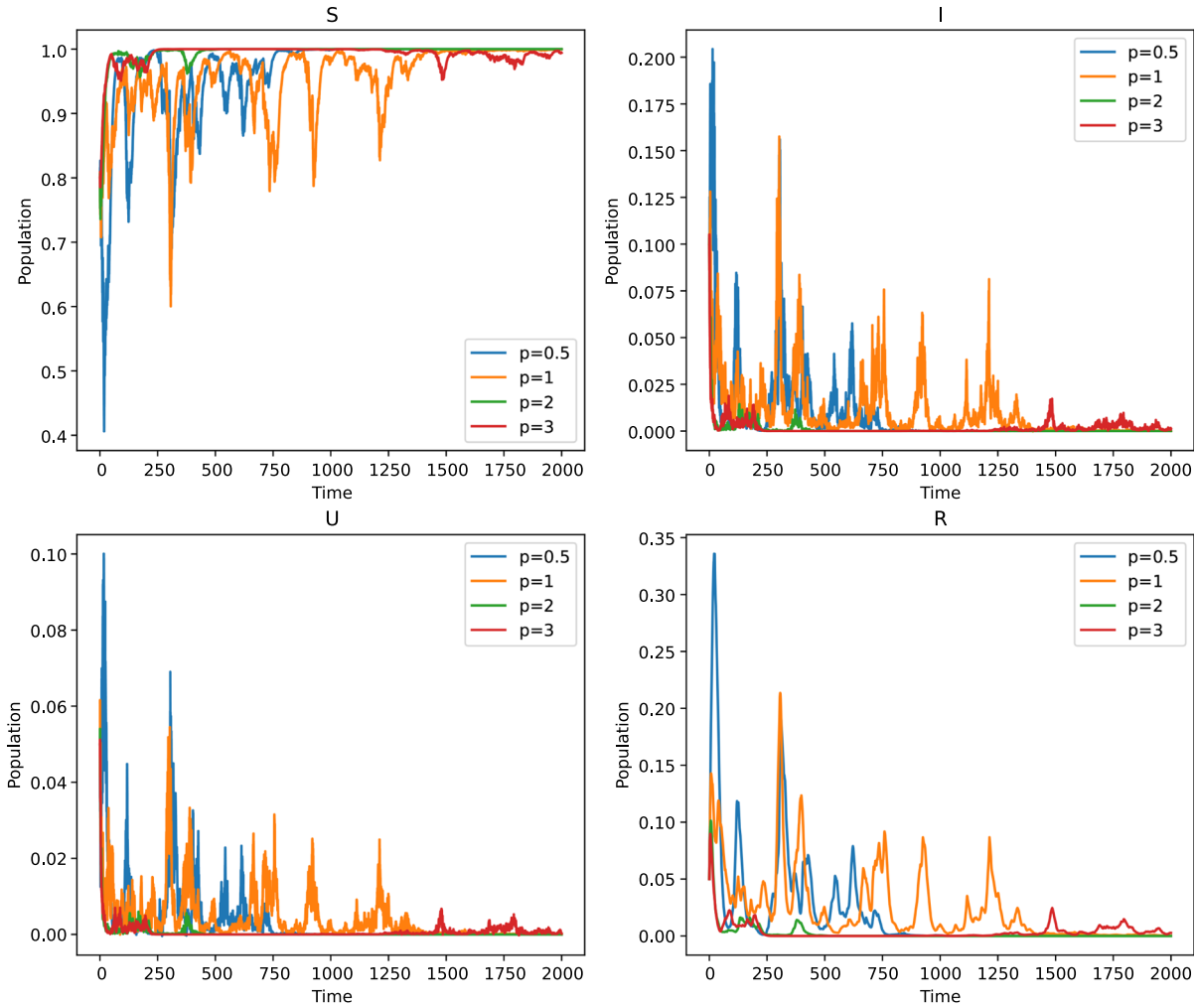


**Fig. 1** The impact of the infection force $p$ on the dynamics of disease transmission $Z(t)$ starting from $z_0 = (0.8, 0.1, 0.05, 0.05)$ when $\mathcal{R}_s < 1$

### 4.1 Synthetic data

We first conduct some numerical simulations are given to both illustrate and validate our theoretical findings with various examples.

#### *4.1.1 Extinction of diseases*

We exemplify the conditions for disease extinction as delineated in Theorem 3 (Fig. 1). By setting the parameters to specific values: $\mu_1 = 0.1$, $\alpha = 0.05$, $\delta = 0.2$, $\omega = 0.02$, $\beta = 0.375$, $\nu = 0.7$, $a = 0.1$, $p \in \{0.5, 1, 2, 3\}$, $\sigma = 0.3$, and considering the function $g(S) = S^p$, it is evident that $M_s = 1$. The conditions for extinction, $\mathcal{R}_s < 1$ and $M_s\sigma^2 < \beta(1+a)^2$, are satisfied, signifying the incapacity of the disease to perpetuate within the populace autonomously. On average, each infected individual transmits the disease to fewer than one other individual during their period of infectivity. Consequently, this trend leads to the gradual decline and ultimate eradication of the disease from the population. Furthermore, it is pertinent to underscore that the augmenting power of the infection force, denoted by parameter $p$, inversely influences the incidence of the disease and its propagation dynamics. As the value of $p$ escalates, the disease incidence diminishes, manifesting in a reduced rate of spread throughout the population. This observation underscores the

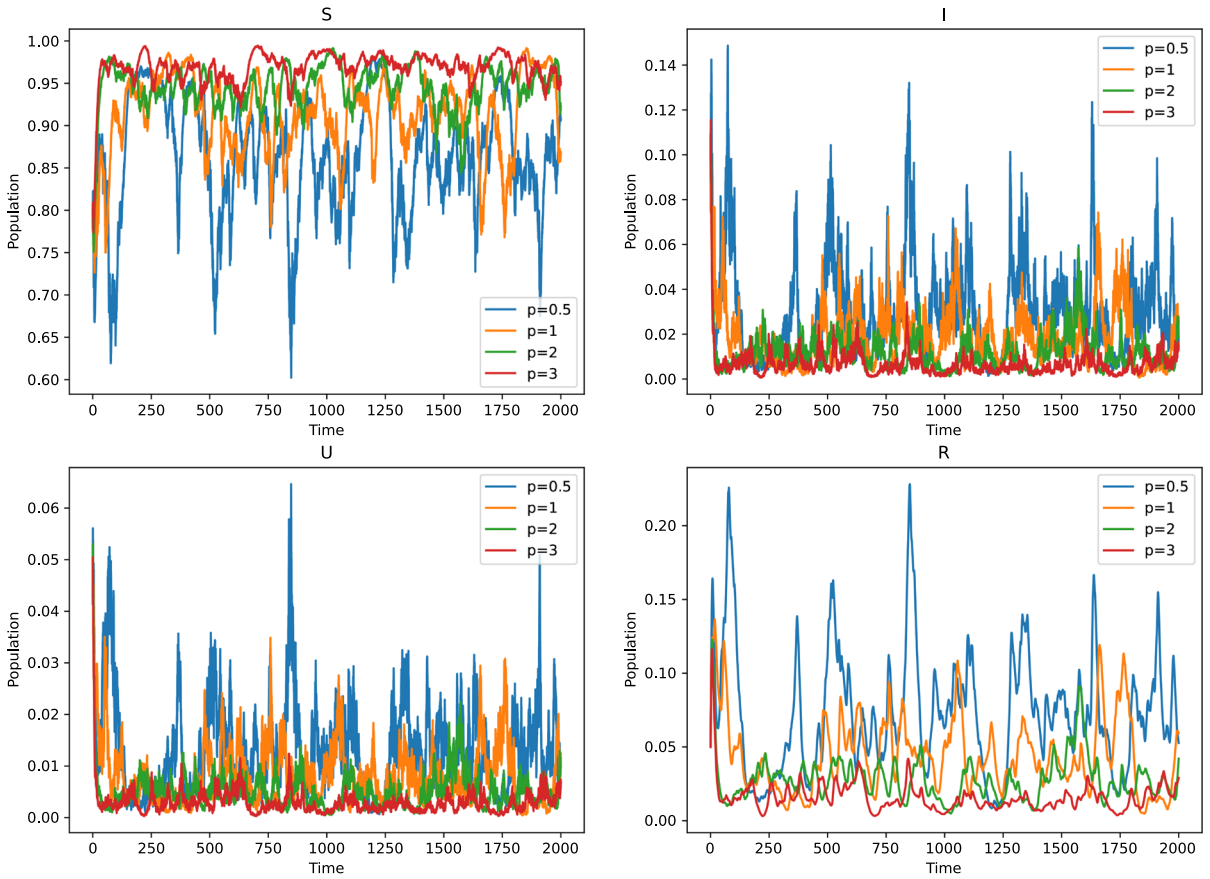


**Fig. 2** The impact of the infection force $p$ on the dynamics of disease transmission $Z(t)$ starting from $z_0 = (0.8, 0.1, 0.05, 0.05)$ when $\mathcal{R}_s > 1$

crucial role of parameter $p$ in modulating the dynamics of disease transmission and underscores its significance in epidemiological modeling and control strategies.

#### *4.1.2 Disease persistence*

In our subsequent analysis, we deliberately select specific parameter configurations to delve into the dynamics of the SIURS epidemic model across varying values of the power parameter, denoted as $p$. Retaining the previously chosen parameter settings and function $g(S)$ from our prior example, we introduce alterations in certain parameters. Specifically, adjusting $\beta = 0.4$, $a = 0.2$, and $\sigma = 0.2$, we derive the basic reproduction number, denoted as $\mathcal{R}_s$, where $\mathcal{R}_s > 1$ and $\beta > \frac{1}{2}\sigma^2 M_s$. This outcome signifies the sustained prevalence of the infectious disease within the population. Notably, this persistence observation resonates with the theoretical insights outlined in Theorem 2, which delineates conditions conducive to the enduring presence of infectious diseases (Fig. 2). Moreover, the system is positively recurrent, exhibiting a unique stationary distribution shown in Fig. 3. Furthermore, consistent with our expectations, as the parameter $p$ escalates, the incidence of the disease diminishes, leading to a discernible reduction in its rate of transmission across the population.

#### *4.1.3 The impact of the susceptible contact function $g(S)$*

In this section, we explore how the choice of the susceptible contact function $g(S)$ affects the behavior of the solution to the system (1). We compare the dynamics resulting from three distinct functions:

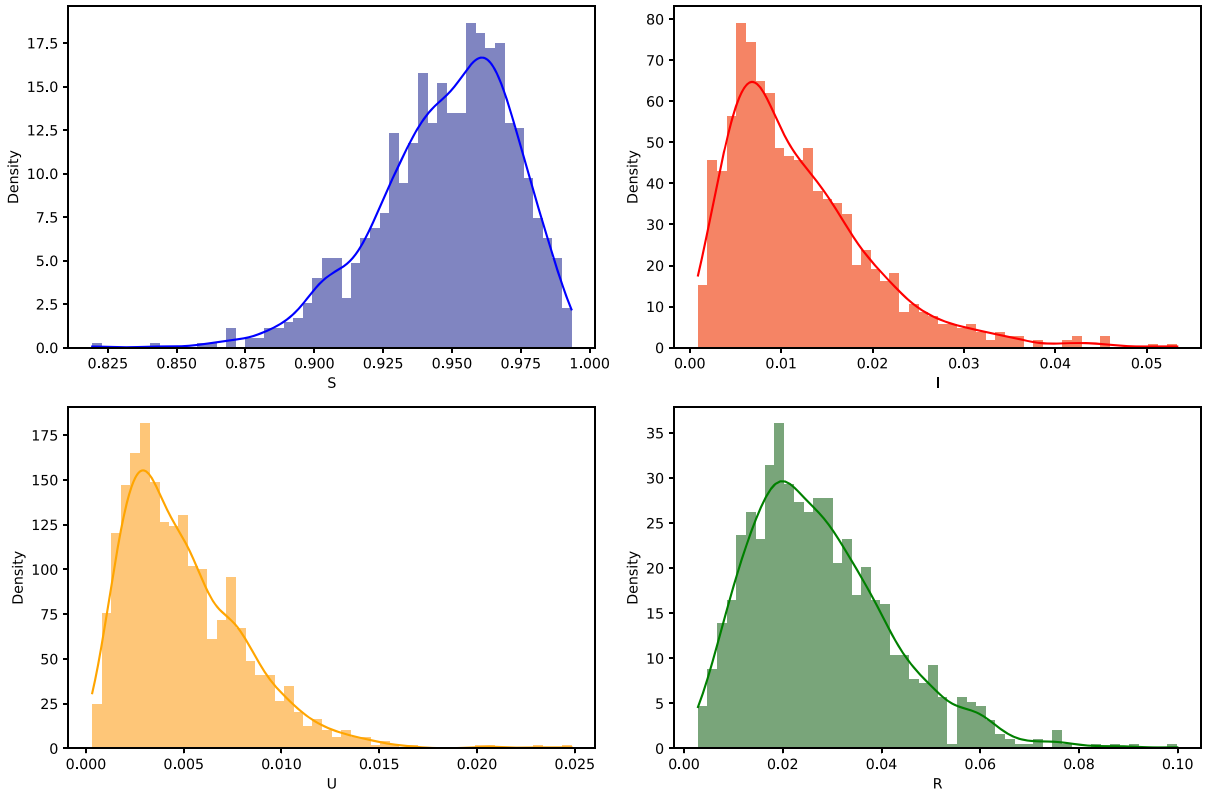


**Fig. 3** The density functions corresponding to $S(t)$, $I(t)$, $U(t)$ and $R(t)$ for $p = 2$ based on 1000 simulations

$$g_1(S) = S^2, \quad g_2(S) = b - be^{-S}, \quad \text{and}$$
$$g_3(S) = \frac{cS}{1+S},$$

where $b$ and $c$ represent positive constants. Table 1 presents the modified parameters for each scenario tested. The remaining parameters are held constant at $\mu_1 = 0.1, \alpha = 0.05, \delta = 0.2, \omega = 0.02, \nu = 0.7$ and $p = 2$.

This study investigates the impact of the choice of the susceptible contact function $g(S)$ on the behavior of the system described by (1). By comparing the dynamics resulting from different functions, we gain insights into how the system responds to variations in $g(S)$, which directly influences the transmission dynamics of the disease (4). The function $g(S)$ plays a crucial role in determining the evolution direction of the epidemic $\mathcal{R}_s$ and the rate at which susceptible individuals become infected. For instance, when $g_1(S) = S^2$, the transmission rate increases quadratically with the susceptible population $S$, potentially leading to rapid disease spread in densely populated regions. On the other hand, $g_2(S) = b - be^{-S}$ introduces a more nuanced transmission pattern, where $b$ controls the initial transmission rate, and the exponential decay term modulates the rate as the susceptible population decreases. This function may represent scenarios where preventive measures are implemented gradually or where the effectiveness of interventions diminishes over time. Moreover, $g_3(S) = \frac{cS}{1+S}$ exhibits a saturating effect on transmission. Initially, the transmission rate increases linearly with $S$, but it eventually saturates as $S$ approaches larger values. This function captures scenarios where the disease transmission reaches a plateau due to factors such as limited contact opportunities or immunity buildup within the population. By analyzing the response of the system (1) to these different $g(S)$ functions, we gain insights into the interplay between population dynamics and disease transmission dynamics. This understanding can inform public health strategies and interventions aimed at controlling the spread of infectious diseases in real-world scenarios. The importance of selecting a susceptible contact function $g(S)$ that accurately captures the dynamics of disease trans-

**Table 1** List of parameters for different scenario tested

| Parameters | Scenario 1 | Scenario 2 | Scenario 3 | Scenario 4 | Scenario 5 | Scenario 6 |
|---|---|---|---|---|---|---|
| $\beta$ | 0.375 | 0.4 | 0.4 | 0.4 | 0.5 | 0.5 |
| $\sigma$ | 0.3 | 0.2 | 0.3 | 0.4 | 0.3 | 0.3 |
| $a$ | 0.1 | 0.1 | 0.1 | 0.2 | 0.2 | 0.2 |
| $b$ | 1 | 1 | 2 | 2 | 1.8 | 1 |
| $c$ | 1 | 1.5 | 1 | 2.5 | 2.5 | 2.5 |
| $\mathcal{R}_{s,1}$ | 0.968 | 1.091 | 1.033 | 0.986 | 1.311 | 1.311 |
| $\mathcal{R}_{s,2}$ | 0.649 | 0.709 | 1.235 | 1.153 | 1.457 | 0.872 |
| $\mathcal{R}_{s,3}$ | 0.522 | 0.835 | 0.557 | 1.145 | 1.567 | 1.567 |

mission cannot be overstated. It directly influences the behavior of the system and the rate at which the disease spreads within a population. Understanding the implications of different $g(S)$ functions is essential for developing effective strategies to control and mitigate the impact of infectious diseases.

In the next section of this study, we will delve deeper into this topic by proposing a selection method for the function $g$. Our objective is to identify the most informative function that provides valuable insights into the interplay between population susceptibility and disease transmission dynamics. Through this analysis, we aim to enhance our understanding of the factors driving disease spread and contribute to the development of more accurate models for predicting and managing infectious disease outbreaks.

#### *4.1.4 Selection method for the susceptible contact function $g(S)$*

In real-world scenarios and public health data analysis, it's common to observe the number of infected and recovered individuals on a daily or weekly basis. Leveraging this insight, we propose a method for selecting the function $g(S)$ by minimizing the Mean Square Error (MSE) between the actual observations and the simulated data using multiple candidate functions $g$. Ultimately, the goal is to identify the function that yields the lowest error, thereby providing the best fit to the observed data. Mathematically, we express this as:

$$MSE(g) = \mathbb{E}\left[(I_{obs} - I_{sim}(g))^2\right] + \mathbb{E}\left[(R_{obs} - R_{sim}(g))^2\right], \tag{15}$$

and

$$g^* = \underset{g \in C^1((0,1),\mathbb{R}^+)}{argmin} \; MSE(g).$$

To achieve this, we generate 1000 paths of the $Z_g(t)$ process described by (1) for $g(S) = S$, starting from $z_0$, with varying horizon times $H$ using the parameters from scenario 1 in Table 1. Next, for each candidate function $g_i(S)$, we simulate $Z_{g_i}$ and estimate the MSE $\varepsilon_H$ using the Monte Carlo method for different values of $H$. In this example, we consider the following set of candidate functions:

$$g_1(S) = S^{1/2}, \quad g_2(S) = S, \quad g_3(S) = S^{3/2}, \quad g_4(S) = S^2, \quad g_5(S) = 1 - e^{-S},$$

and

$$g_6(S) = \frac{S}{1+S}.$$

In summary, the proposed selection method consists of the following 4 steps:

(i) Simulate the system for $g(S) = S$ and record the 1000 trajectories of the $I$ and $R$ compartments (presente the real observations in this case).
(ii) For each candidate function $g_i(S)$ ($i = 1$ to 6), simulate the corresponding system using the same initial conditions and the same parameter values, and record the 1000 trajectories of the $I$ and $R$ compartments.
(iii) Calculate the MSE between simulated and real observations employing Monte Carlo method for each function $g_i(S)$ for different values of $H$.
(iv) Repeat steps 2 and 3 for $H = 100, 500, 1000, 2000$.

As $H$ increases, the Mean Squared Error (MSE) tends to decrease. This observation is consistent with

**Fig. 4** Evolution of $Z(t)$ for different susceptible contact function $g(S)$

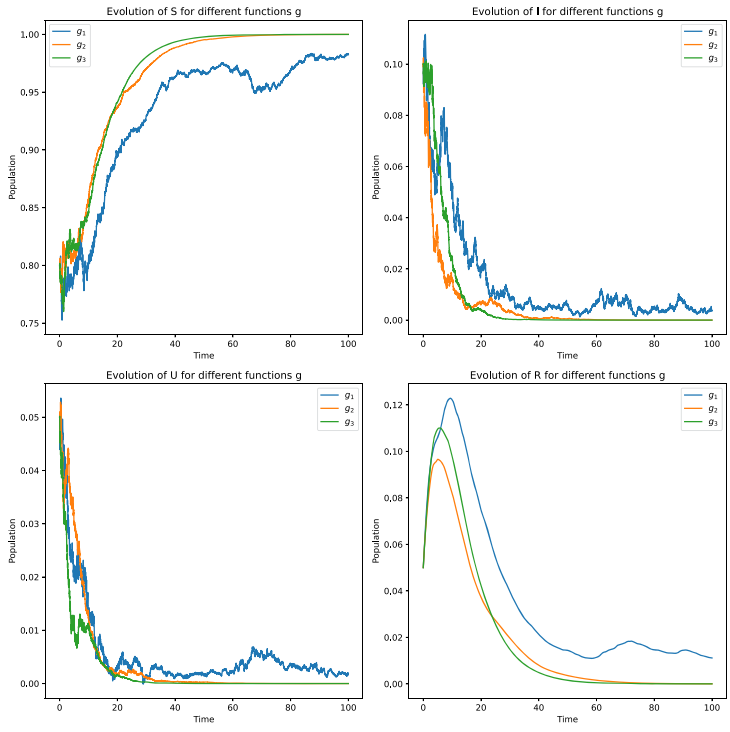


(a) Case 1: $\mathcal{R}_{s,3} < \mathcal{R}_{s,2} < \mathcal{R}_{s,1}$.

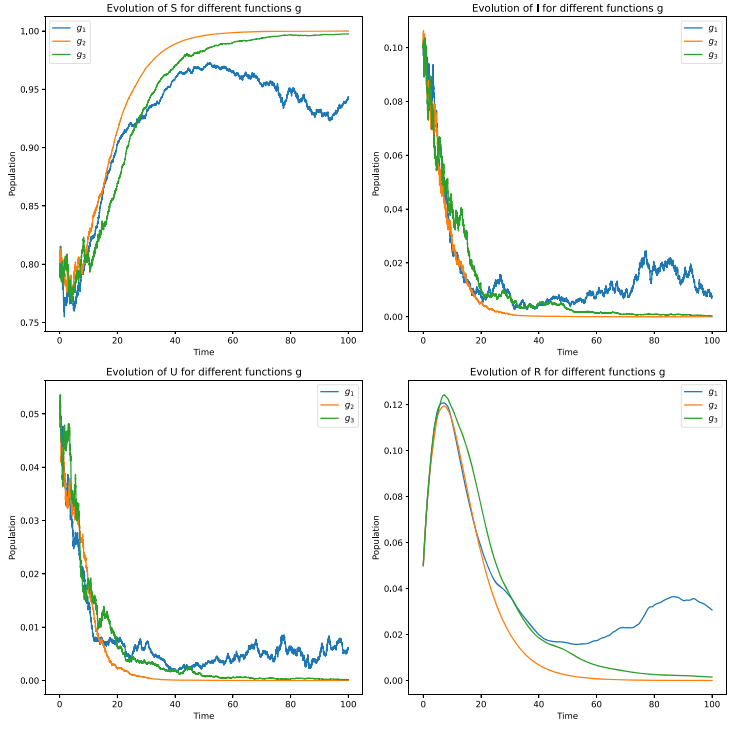


(b) Case 2: $\mathcal{R}_{s,2} < \mathcal{R}_{s,3} < \mathcal{R}_{s,1}$.

**Fig. 4** continued

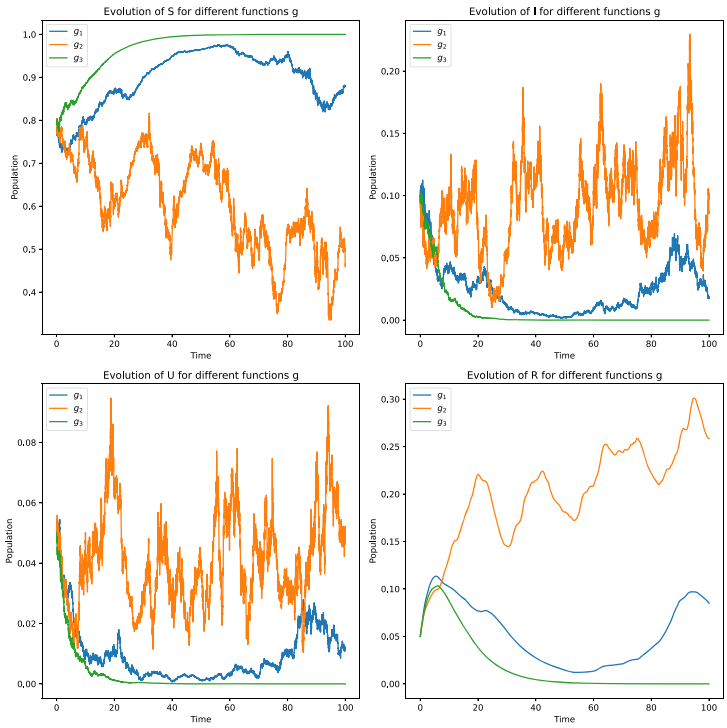


(c) Case 3: $\mathcal{R}_{s,3} < \mathcal{R}_{s,1} < \mathcal{R}_{s,2}$.

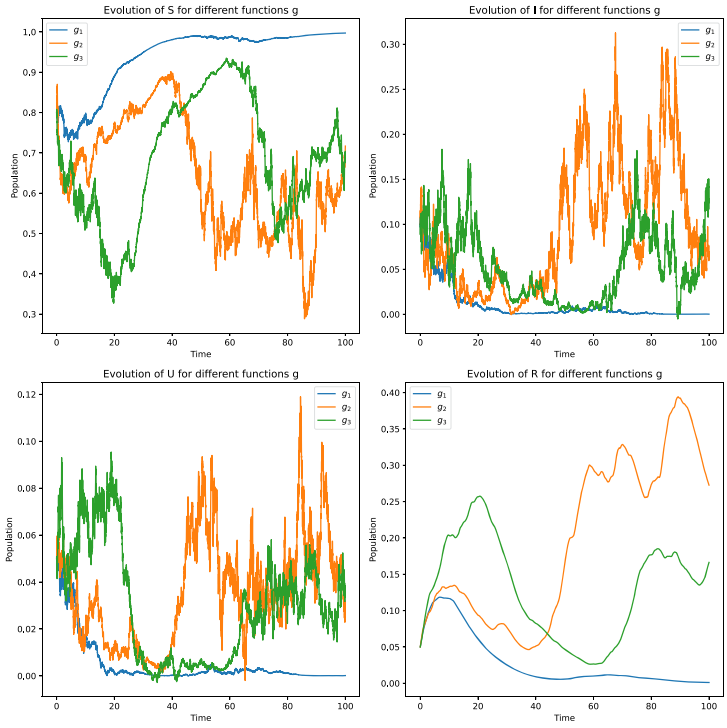


(d) Case 4: $\mathcal{R}_{s,1} < \mathcal{R}_{s,3} < \mathcal{R}_{s,2}$.

**Fig. 4** continued

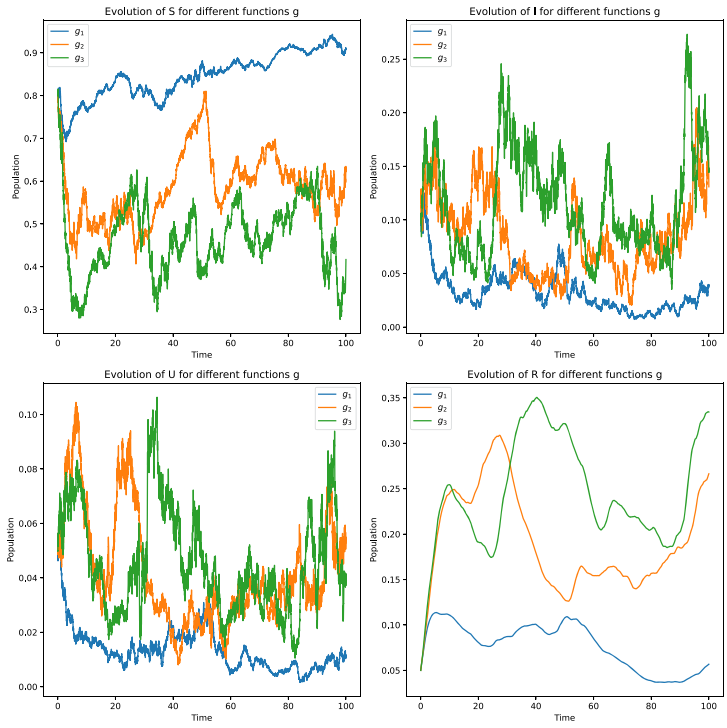


(e) Case 5: $\mathcal{R}_{s,1} < \mathcal{R}_{s,2} < \mathcal{R}_{s,3}$.

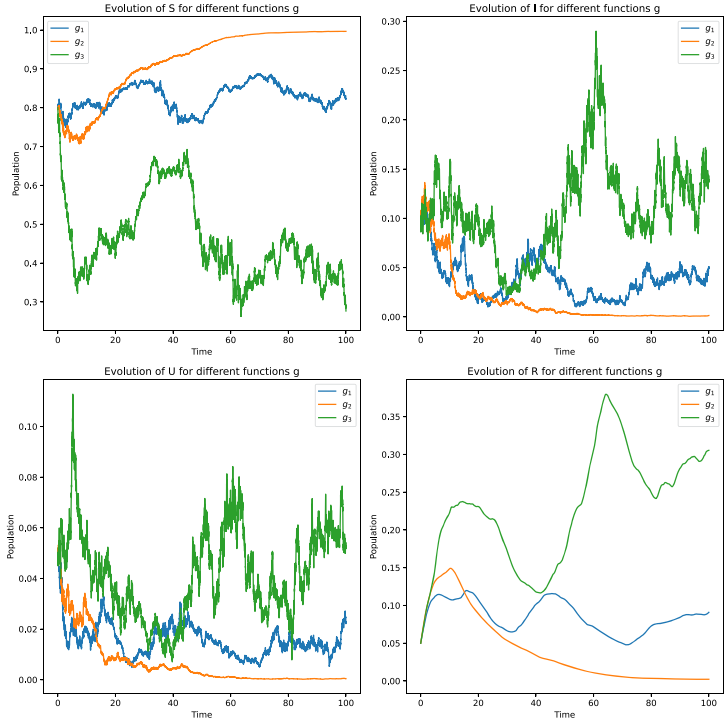


(f) Case 6: $\mathcal{R}_{s,2} < \mathcal{R}_{s,1} < \mathcal{R}_{s,3}$.

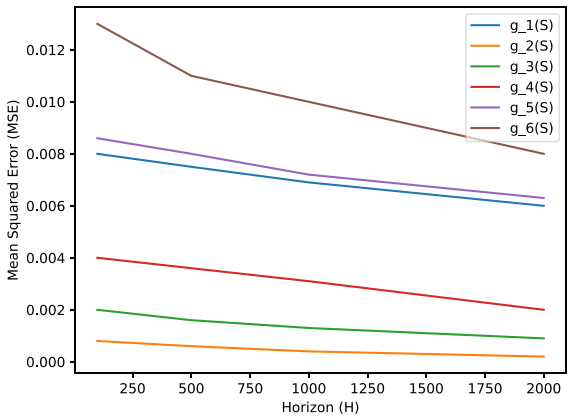


**Fig. 5** MSE $\varepsilon_H$ for different $g(S)$ functions tested

the notion that as we observe the system over a longer time horizon, the simulated trajectories tend to converge towards a more accurate representation of the true dynamics. Additionally, the MSE values indicate that the method effectively selects the most suitable function, $g_2(S)$, as the one with the lowest error across different horizon values (Fig. 5). This suggests that $g_2(S)$ provides the best fit to the observed data and captures the underlying dynamics of the system most accurately among the candidate functions tested.

This approach allows us to choose the $g(S)$ function that most accurately captures the transmission dynamics observed in real-world data. By aligning the simulated outcomes with empirical observations, we can enhance the predictive power of our models and better understand the underlying mechanisms driving disease transmission. This selection method facilitates the development of more reliable and informative models for studying and managing infectious diseases.

### 4.2 COVID-19 data in the UK

COVID-19, caused by the Severe Acute Respiratory Syndrome Coronavirus 2 (SARS-CoV-2), has emerged as one of the most significant health crises of the twenty-first century worldwide [31,33,34]. Originating in Wuhan, China, in late 2019, the outbreak swiftly spread across the globe, prompting the World Health Organization (WHO) to declare it a global pandemic on March 11, 2020 [35]. In the United Kingdom (UK), the first cases were identified on January 31, 2020, marking the onset of a rapid escalation in cases throughout February and March [36]. By December 2020, the UK had endured over 50, 000 deaths and 230, 000 hospital admissions due to COVID-19, despite estimates suggesting that less than 20% of the population had been exposed to the virus. As of December 31, 2020, the population of the UK stood at 68, 602, 259, serving as the initial value for the susceptible population in epidemiological modeling [37]. The birth rate was estimated at 2371 per day [37], contributing to the constant influx of individuals into the susceptible class.

Now, we rigorously calibrated our SIURS model to capture the temporal dynamics of daily new reported cases of SARS-CoV-2 and hospital admissions in the UK, covering the period from January 31, 2020, to May 20, 2022 [38] (Fig. 5). During this timeframe, the highest number of reported infections peaked at 226, 524 individuals in March 2022, with an average of 25, 587.23 daily infections and 10, 053.23 daily hospital admissions in the UK.

One of the central hurdles in mathematical modeling studies is the precise estimation of model parameters. By scrutinizing available literature, clinical studies and research investigating the progression of the COVID-19 pandemic in the UK, we have derived estimates for specific model parameters. Table 2 provides these estimates along with their respective sources.

To address the remaining parameters, namely $a$ and the function $g$, we opt for a systematic approach. We employ the power function $g(S) = S^p$ and explore a range of values for the exponent $p$ from 0 to 10, and for the parameter $a$ from 0 to 2. This selection process aligns with the methodology outlined in Sect. 4.1.4, where we use a fitting procedure to calibrate the model against observed daily COVID-19 incidences and hospital cases. The objective is to locally minimize the Mean Squared Error (MSE), thus refining the accuracy of the model. The optimal values of $p$ and $a$ that yield the lowest MSE (15) are found to be $p = 1.3$ and $a = 0.85$.

Upon fitting our stochastic SIURS model to real data (Fig. 7), we observe that the results accurately capture the modeled trends, especially in the initial stages of the pandemic (from January 30, 2020, to mid-2021). However, significant deviations between the adjusted data and observations become apparent thereafter. This phenomenon can be attributed to the emergence of new variants of SARS-CoV-2. These disparities arise due to multifaceted intricacies inherent in modeling COVID-19. These variations stem from multiple factors, including the natural variability in human behavior, the evolv-

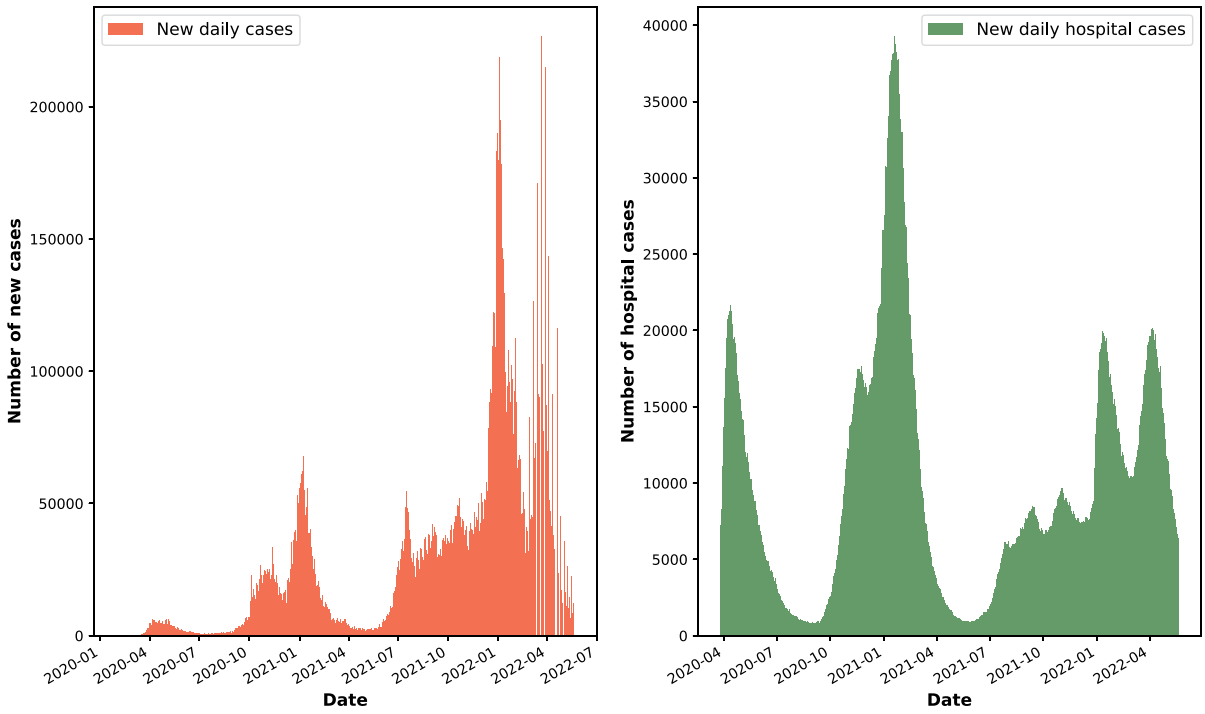


**Fig. 6** New daily reported cases and hospital admissions in the UK (31/01/2020–20/05/2022)

**Table 2** List of parameters values for the SIURS model (1) of COVID-19 transmission in the UK based on model calibration, relevant literature and clinical studies

| Parameters | Interpretation | Value (Unit) | Likely range | Source |
|---|---|---|---|---|
| $\mu_1$ | Natural death rate | 10.45/1000 | 8.7/1000–12.2/1000 | [39] |
| $\beta$ | Infectious contact rate | 0.5 day$^{-1}$ | 0.2–1.5 | [40–42] |
| $\omega$ | Losing immunity rate | 0.002 day$^{-1}$ | 0.0008–0.004 | [43,44] |
| $\alpha$ | Disease-induced death rate | 0.015 day$^{-1}$ | 0.001–0.1 | [41,45] |
| $\delta$ | Recovery rate | 0.15 day$^{-1}$ | 0.032–0.032 | [46–48] |
| $\nu$ | Proportion of infections reported | 0.7 | 0.5–1 | [36,49] |

ing nature of health interventions over time, and the inherent dynamics of virus transmission. Moreover, there are latent variables whose effects on the trajectory of the epidemic are not fully understood, adding further complexity. Additionally, spatial factors such as population density, patterns of inter-regional mobility, and differences in intervention strategies between regions contribute additional layers of complexity to the situation. Furthermore, the stochastic nature of the disease process, combined with potential flaws or gaps in data collection, amplifies these discrepancies. Despite these challenges, our model represents a significant step forward in understanding disease dynamics, offering valuable insights for future analyses and the development of more effective strategies for managing the pandemic.

## 5 Conclusion and perspectives

In conclusion, our study offers a comprehensive analysis of a stochastic epidemiological model that integrates unreported cases and incorporates a general susceptible contact function. We have highlighted the pivotal role of the critical threshold parameter in determining the long-term dynamics of infectious diseases. By con-

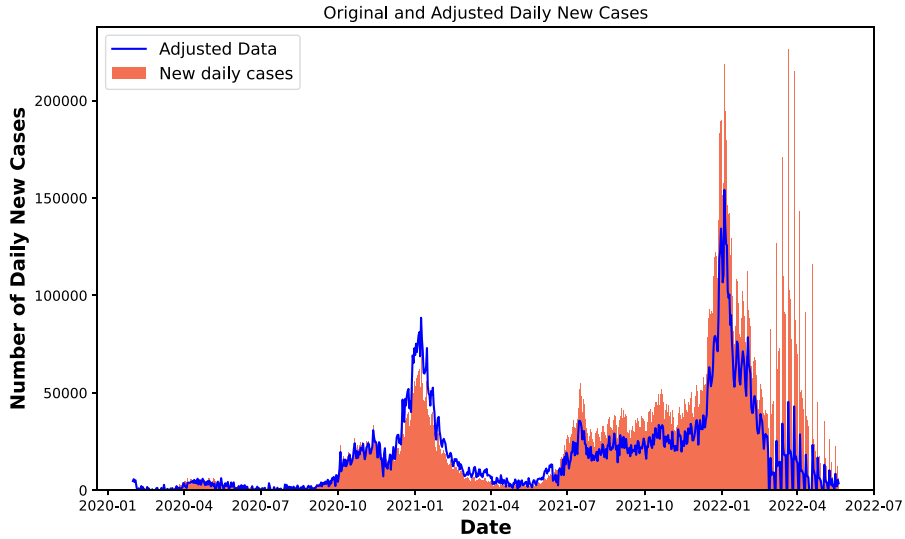


**Fig. 7** The model (1) fitted curve compared to reported COVID-19 cases in the UK: January 31, 2020, to May 20, 2022

ducting extensive numerical simulations and calibrating the model with real-world data from the UK, we have demonstrated its robustness in accurately capturing phenomena such as disease extinction and persistence. Our findings emphasize the critical influence of the susceptible contact function $g(S)$ in optimizing the model's predictive accuracy for practical applications.

Further research for this work could explore the effectiveness of various intervention strategies, such as vaccination campaigns, social distancing measures, and healthcare capacity improvements. By simulating the effect of these interventions in the version, researchers can gain treasured insights into their potential to mitigate the spread of infectious illnesses and inform evidence-primarily based choice-making in public health policy. Moreover, extending the model to encompass multiple geographic regions or populations could permit the analysis of local disparities in disease transmission and intervention effectiveness. This extension ought to empower policymakers to tailor interventions to precise neighborhood contexts, allocate resources extra correctly, and deal with the specific challenges faced via distinctive groups. Additionally, investigating the long-term dynamics and evolutionary methods of infectious diseases, such as the emergence of latest variants, holds significant promise for boosting our information of epidemic trajectories. By integrating evolutionary modeling strategies into the framework, researchers can more accurately predict and respond to emerging infectious disease threats, in the end contributing to the development of more resilient public health techniques.

**Author contributions** IB Writing-review and editing, Writing-original draft, Visualization, Validation, Software, Resources, Methodology, Investigation, Formal analysis, Data curation, Conceptualization.

**Funding** No funding was received.

**Data availability** The data used for the research described in the article came from [36].

**Declarations**

**Conflict of interest** The authors declare that they have no known competing financial interests or personal relationships that could have appeared to influence the work reported in this paper.

## References

1. Hethcote, H.W.: The mathematics of infectious diseases. SIAM Rev. **42**(4), 599–653 (2000)
2. Allen, L.J.: A primer on stochastic epidemic models: formulation, numerical simulation, and analysis. Infect. Dis. Model. **2**(2), 128–142 (2017)
3. Heesterbeek, H.: The law of mass-action in epidemiology: a historical perspective. In: Ecological Paradigms Lost: Routes of Theory Change, pp. 81–104 (2005)
4. Melegaro, A., Jit, M., Gay, N., Zagheni, E., Edmunds, W.J.: What types of contacts are important for the spread of infections? using contact survey data to explore European mixing patterns. Epidemics **3**(3–4), 143–151 (2011)
5. Mousa, A., Winskill, P., Watson, O.J., Ratmann, O., Monod, M., Ajelli, M., Diallo, A., Dodd, P.J., Grijalva, C.G., Kiti, M.C., et al.: Social contact patterns and implications for

infectious disease transmission-a systematic review and meta-analysis of contact surveys. Elife **10**, 70294 (2021)
6. Hossain, A.D., Jarolimova, J., Elnaiem, A., Huang, C.X., Richterman, A., Ivers, L.C.: Effectiveness of contact tracing in the control of infectious diseases: a systematic review. The Lancet Public Health (2022)
7. Müller, J., Kretzschmar, M.: Contact tracing-old models and new challenges. Infect. Dis. Model. **6**, 222–231 (2021)
8. Aronson, J.K., Ferner, R.E.: The law of mass action and the pharmacological concentration-effect curve: resolving the paradox of apparently non-dose-related adverse drug reactions. Br. J. Clin. Pharmacol. **81**(1), 56–61 (2016)
9. Cao, F., Lü, X., Zhou, Y.-X., Cheng, X.-Y.: Modified seiar infectious disease model for omicron variants spread dynamics. Nonlinear Dyn. **111**(15), 14597–14620 (2023)
10. Yin, Q., Wang, Z., Xia, C.: Information-epidemic coevolution propagation under policy intervention in multiplex networks. Nonlinear Dyn. **111**(15), 14583–14595 (2023)
11. Guo, H., Yin, Q., Xia, C., Dehmer, M.: Impact of information diffusion on epidemic spreading in partially mapping two-layered time-varying networks. Nonlinear Dyn. **105**(4), 3819–3833 (2021)
12. Shulgin, B., Stone, L., Agur, Z.: Pulse vaccination strategy in the sir epidemic model. Bull. Math. Biol. **60**(6), 1123–1148 (1998)
13. Zhou, L., Fan, M.: Dynamics of an sir epidemic model with limited medical resources revisited. Nonlinear Anal. Real World Appl. **13**(1), 312–324 (2012)
14. Bouzalmat, I., El Idrissi, M., Settati, A., Lahrouz, A.: Stochastic sirs epidemic model with perturbation on immunity decay rate. J. Appl. Math. Comput. **69**(6), 4499–4524 (2023)
15. Kabir, K.A., Kuga, K., Tanimoto, J.: Analysis of sir epidemic model with information spreading of awareness. Chaos, Solitons Fractals **119**, 118–125 (2019)
16. Lahrouz, A., Settati, A.: Necessary and sufficient condition for extinction and persistence of sirs system with random perturbation. Appl. Math. Comput. **233**, 10–19 (2014)
17. Lahrouz, A., Omari, L.: Extinction and stationary distribution of a stochastic sirs epidemic model with non-linear incidence. Stat. Probab. Lett. **83**(4), 960–968 (2013)
18. Tornatore, E., Buccellato, S.M., Vetro, P.: Stability of a stochastic sir system. Physica A **354**, 111–126 (2005)
19. Lan, G., Chen, Z., Wei, C., Zhang, S.: Stationary distribution of a stochastic siqr epidemic model with saturated incidence and degenerate diffusion. Physica A **511**, 61–77 (2018)
20. Wang, W., Gao, X., Cai, Y., Shi, H., Fu, S.: Turing patterns in a diffusive epidemic model with saturated infection force. J. Franklin Inst. **355**(15), 7226–7245 (2018)
21. Li, X., Cai, Y., Wang, K., Fu, S., Wang, W.: Non-constant positive steady states of a host-parasite model with frequency-and density-dependent transmissions. J. Franklin Inst. **357**(7), 4392–4413 (2020)
22. Ji, C.: The threshold for a stochastic hiv-1 infection model with beddington-deangelis incidence rate. Appl. Math. Model. **64**, 168–184 (2018)
23. Salman, S.M.: A nonstandard finite difference scheme and optimal control for an hiv model with beddington-deangelis incidence and cure rate. Eur. Phys. J. Plus **135**, 1–23 (2020)
24. Jan, M.N., Ali, N., Zaman, G., Ahmad, I., Shah, Z., Kumam, P.: Hiv-1 infection dynamics and optimal control with crowley-martin function response. Comput. Methods Prog. Biomed. **193**, 105503 (2020)
25. Imhof, L., Walcher, S.: Exclusion and persistence in deterministic and stochastic chemostat models. J. Differ. Equ. **217**(1), 26–53 (2005)
26. Nguyen, D.H., Nguyen, N.N., Yin, G.: General nonlinear stochastic systems motivated by chemostat models: complete characterization of long-time behavior, optimal controls, and applications to wastewater treatment. Stoch. Proces. Their Appl. **130**(8), 4608–4642 (2020)
27. Nguyen, D.H., Yin, G.: Stability of regime-switching diffusion systems with discrete states belonging to a countable set. SIAM J. Control. Optim. **56**(5), 3893–3917 (2018)
28. Bellet, L.R.: In: Attal, S., Joye, A., Pillet, C.-A. (eds) Ergodic Properties of Markov Processes, pp. 1–39. Springer, Berlin, Heidelberg (2006). https://doi.org/10.1007/3-540-33966-3_1
29. Tuominen, P., Tweedie, R.L.: Subgeometric rates of convergence of f-ergodic Markov chains. Adv. Appl. Probab. **26**(3), 775–798 (1994)
30. Zhao, Y., Jiang, D.: The threshold of a stochastic sis epidemic model with vaccination. Appl. Math. Comput. **243**, 718–727 (2014)
31. Caraballo, T., Bouzalmat, I., Settati, A., Lahrouz, A., Brahim, A.N., Harchaoui, B.: Stochastic covid-19 epidemic model incorporating asymptomatic and isolated compartments. In: Mathematical Methods in the Applied Sciences (2024)
32. Higham, D.J.: An algorithmic introduction to numerical simulation of stochastic differential equations. SIAM Rev. **43**(3), 525–546 (2001)
33. Shereen, M.A., Khan, S., Kazmi, A., Bashir, N., Siddique, R.: Covid-19 infection: emergence, transmission, and characteristics of human coronaviruses. J. Adv. Res. **24**, 91–98 (2020)
34. Yin, M.-Z., Zhu, Q.-W., Lü, X.: Parameter estimation of the incubation period of covid-19 based on the doubly interval-censored data model. Nonlinear Dyn. **106**(2), 1347–1358 (2021)
35. World Health Organization (WHO). Corona Virus Disease (COVID-19) Outbreak Situation. World Health Organization (2020). https://www.who.int/emergencies/diseases/novel-coronavirus-2019
36. https://www.gov.uk/government/publications/health-protection-report-volume-14-2020
37. https://countrymeters.info/en/United_Kingdom_(UK)
38. https://ukhsa-dashboard.data.gov.uk
39. https://www.statista.com/statistics/281478/death-rate-united-kingdom-uk/
40. Li, R., Pei, S., Chen, B., Song, Y., Zhang, T., Yang, W., Shaman, J.: Substantial undocumented infection facilitates the rapid dissemination of novel coronavirus (sars-cov-2). Science **368**(6490), 489–493 (2020)
41. Crellen, T., Pi, L., Davis, E.L., Pollington, T.M., Lucas, T.C., Ayabina, D., Borlase, A., Toor, J., Prem, K., Medley, G.F., et al.: Dynamics of sars-cov-2 with waning immunity in the UK population. Philos. Trans. R. Soc. B **376**(1829), 20200274 (2021)
42. Nabi, K.N.: Forecasting covid-19 pandemic: a data-driven analysis. Chaos, Solitons Fractals **139**, 110046 (2020)

43. Cao, W.-C., Liu, W., Zhang, P.-H., Zhang, F., Richardus, J.H.: Disappearance of antibodies to sars-associated coronavirus after recovery. N. Engl. J. Med. **357**(11), 1162–1163 (2007)
44. Rosado, J., Pelleau, S., Cockram, C., Merkling, S.H., Nekkab, N., Demeret, C., Meola, A., Kerneis, S., Terrier, B., Fafi-Kremer, S., et al.: Multiplex assays for the identification of serological signatures of sars-cov-2 infection: an antibody-based diagnostic and machine learning study. Lancet Microbe **2**(2), 60–69 (2021)
45. Moya-Salazar, J., Cañari, B., Zuñiga, N., Jaime-Quispe, A., Rojas-Zumaran, V., Contreras-Pulache, H.: Deaths, infections, and herd immunity in the covid-19 pandemic: a comparative study of the strategies for disease containment implemented in peru and the united kingdom. Revista de la Facultad de Medicina **70**(2) (2022)
46. He, X., Lau, E.H., Wu, P., Deng, X., Wang, J., Hao, X., Lau, Y.C., Wong, J.Y., Guan, Y., Tan, X., et al.: Temporal dynamics in viral shedding and transmissibility of covid-19. Nat. Med. **26**(5), 672–675 (2020)
47. Li, Q., Guan, X., Wu, P., Wang, X., Zhou, L., Tong, Y., Ren, R., Leung, K.S., Lau, E.H., Wong, J.Y., et al.: Early transmission dynamics in Wuhan, China, of novel coronavirus-infected pneumonia. N. Engl. J. Med. **382**(13), 1199–1207 (2020)
48. Davies, N., Kucharski, A., Eggo, R., Gimma, A., Edmunds, W., Jombart, T., et al.: Effects of non-pharmaceutical interventions on COVID-19 cases, deaths, and demand for hospital services in the UK: a modelling study. Lancet Public Health. **5**(7), e375-85 (2020)
49. https://ourworldindata.org/grapher/uk-cumulative-covid-deaths-rate